Journal of the Mechanics and Physics of Solids 62 (2014) 181–193

Contents lists available at ScienceDirect

Journal of the Mechanics and Physics of Solids

journal homepage: www.elsevier.com/locate/jmps

Stress dependence of cross slip energy barrier for face-centered cubic nickel

Keonwook Kang [a], Jie Yin [b], Wei Cai [b,c,*]

[a] Department of Mechanical Engineering, Yonsei University, Seoul 120-749, South Korea
[b] Department of Materials Science and Engineering, Stanford University, Stanford, United States
[c] Department of Mechanical Engineering, Stanford University, Stanford, CA 94305, United States

ARTICLE INFO

Article history:
Received 8 April 2013
Received in revised form
17 September 2013
Accepted 28 September 2013
Available online 11 October 2013

Keywords:
Dislocation
Cross slip
Line tension model
Atomistic model

ABSTRACT

The energy barrier for the cross slip of screw dislocations in face-centered cubic (FCC) nickel as a function of multiple stress components is predicted by both continuum line tension and discrete atomistic models. Contrary to Escaig's claim that the Schmid stress component has a negligible effect on the energy barrier, we find that the line tension model, when solved numerically, predicts comparable effects from the Schmid stress and the Escaig stress on the cross slip plane. When the line tension model is compared against an atomistic model for FCC nickel, a good agreement is found for the effect of the Escaig stress on the glide plane. However, the atomistic model predicts a stronger effect than the line tension model for the two stress components on the cross slip plane. This discrepancy is larger at higher stresses and is also more severe for the Escaig stress component than for the Schmid stress component.

1. Introduction

Cross slip is the change of slip plane for screw dislocations, usually under stress and with the assistance of thermal fluctuation. It is a fundamental process in the dislocation dynamics of face-centered cubic (FCC) metals (Puschl, 2002). It is believed to be responsible for dynamic recovery in Stage III (Jackson, 1985) and dislocation multiplication and patterning in fatigue (Suresh, 2004). Because cross slip is a thermally activated process, the cross slip rate is controlled by the activation barrier, which depends on the local configuration and the stress state at the screw dislocation. The rate of cross slip as a function of the local stress is an important material-specific input module to dislocation dynamics (DD) simulations (Bulatov and Cai, 2006; Arsenlis et al., 2007), which aim to provide a quantitative link between dislocation mechanisms and constitutive behavior of single crystals.

Identifying the controlling mechanism and quantifying the energy barrier for cross slip has been the motivation of much research over the last two decades. Unfortunately, our present understanding is still far from complete. Extrinsic effects, such as existing jogs (Vegge et al., 2001) and intersection with other dislocations (Washburn, 1965; Rao et al., 2010), are known to influence the activation barrier. Yet, much still remains to be understood even in the idealized case of "homogeneous" cross slip of an isolated, straight screw dislocation, specifically on how the cross slip mechanism and rate depend on stress, temperature and material parameters (such as stacking fault energy). The scope of this paper is limited to the case of "homogeneous" cross slip of isolated straight dislocations.

A variety of mechanisms have been proposed for "homogeneous" cross slip (Puschl, 2002), four of which are briefly mentioned below. The original Schoeck–Seeger–Wolf (SSW) model assumed the cross-slipped segment to be non-dissociated,

* Corresponding author at: Department of Mechanical Engineering, Stanford University, Stanford, CA 94305, United States. Tel.: +1 650 736 1671; fax: +1 650 725 1587.
E-mail address: caiwei@stanford.edu (W. Cai).

0022-5096/$ - see front matter © 2013 Elsevier Ltd. All rights reserved.
http://dx.doi.org/10.1016/j.jmps.2013.09.023

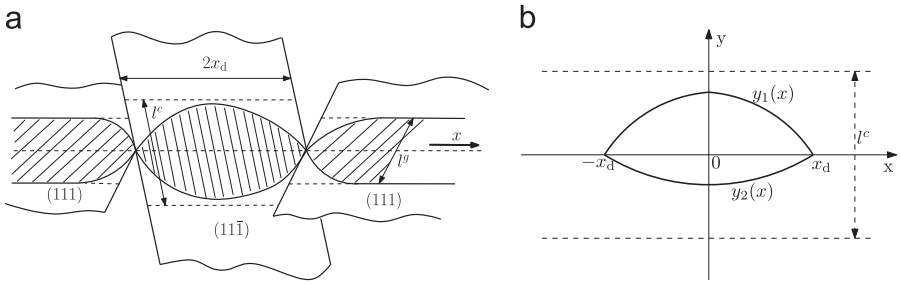

Fig. 1. (a) TheFriedel–Escaig mechanism of cross slip (Puschl, 2002). (b) Two partials on the cross slip plane are described by $y_1(x)$ and $y_2(x)$. In general $y_1(x) \neq -y_2(x)$. The two constriction nodes correspond to $y_1(\pm x_d) = y_2(\pm x_d) = 0$.

which leads to a very high activation barrier, and was later deemed to be irrelevant for FCC metals. In the Friedel–Escaig (FE) model, the cross slipped segment also dissociates in its saddle configuration, as illustrated in Fig. 1(a). The experiments by Bonneville and Escaig (1979) and Bonneville et al. (1988) favor the FE model over the SSW model, but other competing mechanisms also exist. In the Fleischer mechanism, the stacking fault extends into the cross-slip plane without being completely constricted to a point on the glide plane. The saddle configuration contains partial dislocations on both the glide and the cross-slip planes, as well as a stair-rod dislocation at their intersection. Atomistic simulations indicate that this mechanism dominates in the low temperature, high-stress limit (Cai et al., 2004). In the jog-pair mechanism, the dislocation cross-slips back and dissociates on the new glide plane parallel to the original glide plane (i.e. double cross slip). A pair of jogs are created on the segments connecting the two planes. This mechanism is more likely to operate at the high temperature, low-stress limit. In this paper, we will focus mainly on the stress condition where the FE mechanism dominates.

The mechanism and the rate of cross slip is affected by multiple components of the stress tensor. On the cross slip plane, the shear stress parallel to the Burgers vector moves both partials in the same direction, and is called the Schmid stress (σ_s^c). The shear stress perpendicular to the Burgers vector expands or shrinks the stacking fault area, and is called the Escaig stress (σ_e^c). On the (original) glide plane, the Schmid stress (σ_s^g) and Escaig stress (σ_e^g) can be similarly defined. In this paper, we assume that the screw dislocation under consideration does not move on its glide plane, i.e. $\sigma_s^g = 0$. Hence the activation barrier E_b of cross-slip depends on three stress components (σ_s^c, σ_e^c, σ_e^g). Function $E_b(\sigma_s^c, \sigma_e^c, \sigma_e^g)$ is a material-specific input to a DD model for FCC metals. In the framework of multi-scale materials modeling, this function should be constructed from more fundamental, atomistic models. This work is a step towards constructing a function $E_b(\sigma_s^c, \sigma_e^c, \sigma_e^g)$ that is calibrated against atomistic models.

The various models for cross slip can be grouped into three categories: (1) line tension models (Escaig, 1968), (2) linear-elasticity models (Martinez et al., 2008; Ramirez et al., 2012), and (3) atomistic simulations (Vegge et al., 2001; Rasmussen et al., 1997; Rao et al., 1999). In the line-tension model, Escaig (1968) assumed the FE mechanism and made the conclusion that the Schmid stress on the cross-slip plane (σ_s^c) has a negligible effect on the energy barrier. This conclusion has a significant influence on subsequent works, e.g. by directing the focus of atomistic studies to Escaig stresses (Rao et al., 1999). The conclusion that Schmid stress has a negligible effect is in contradiction with a later study (Puschl and Schoeck, 1993) based on the Peierls–Nabarro model, in which σ_s^c and σ_e^c are found to have comparable effects on the activation barrier. The goal of this work is to answer two questions concerning this controversy: (1) Is Escaig's conclusion regarding the negligible effect of Schmid stress justified within the line tension model itself? (2) How good is the line tension approximation when compared with the more fundamental, atomistic model in terms of the stress dependence of the energy barrier? The first question is concerned with the accurate solution of the line model, while the second question is concerned with the physical validity of the line tension model.

The remaining of this paper is organized as follows. In Section 2, we present Escaig's line tension model within a variational formulation. This allows us to solve the line tension model numerically, using an efficient minimization algorithm, without having to invoke the approximations used by Escaig. We find that the line tension model predicts similar effects for σ_s^c and σ_e^c. In Section 3, we present atomistic calculations of cross-slip energy barrier for FCC Ni using an embedded-atom method (EAM) potential. We also describe how the various parameters in the line tension model, such as elastic constants and line energy, are determined by the atomistic model. This approach leaves little room for free adjustable parameters in the line tension model, thus enabling a meaningful test of the line tension approximation. A summary and an outlook for future research are presented in Section 4.

2. Line tension model

2.1. Variational formulation

Escaig's line tension model for cross slip (Escaig, 1968) was based on the earlier work of Stroh on the constriction of dissociated dislocations (Stroh, 1954). In the following, Escaig's model is introduced using a variational formulation, which is physically equivalent to Escaig's original formulation, but is more convenient to use for numerical methods.

In the Friedel–Escaig (FE) mechanism of cross-slip, illustrated in Fig. 1(a), a screw dislocation originally dissociated onto the (111) glide plane (to be designated by superscript ^{g}) has a section dissociated onto the cross slip $(11\bar{1})$ plane (to be designated by superscript ^{c}). Two constriction nodes are formed at the ends of the cross-slipped segment. The two constriction nodes move apart as cross-slip proceeds. In Escaig's model, the energy barrier for cross slip is the maximum energy as a function of the separation between the two constriction nodes.

We shall assume that the dislocation does not move on the (original) glide plane, because the Schmid stress on it is zero, $\sigma_s^g = 0$. Hence the dislocation can reach an equilibrium (meta-stable) state when it is entirely dissociated on the glide plane. The equilibrium separation between the two partials is (Cai et al., 2004)

$$l^g = \frac{A}{F^g} \tag{1}$$

where for a screw dislocation dissociated into two 30° partials (Cai et al., 2000),

$$A = \left(\frac{1}{4} - \frac{1}{12(1-\nu)}\right)\frac{\mu b^2}{2\pi} \tag{2}$$

$$F^g = \gamma_{SF} - b\sigma_e^g/(2\sqrt{3}) \tag{3}$$

μ is the shear modulus, ν is Poisson's ratio, and b is the Burgers vector of the perfect screw dislocation. Hence the sign of the Escaig stress is defined in such a way that a positive σ_e^g increases the equilibrium separation l^g between partials on the glide plane.

Similarly, if the Schmid stress on the cross slip plane is zero, i.e. $\sigma_s^c = 0$, then the dislocation may also exist in an equilibrium (meta-stable) state when it is entirely dissociated on the cross-slip plane, with an equilibrium separation between the two partials equal to

$$l^c = \frac{A}{F^c} \tag{4}$$

where

$$F^c = \gamma_{SF} - b\sigma_e^c/(2\sqrt{3}) \tag{5}$$

Again, a positive σ_e^c increases the equilibrium separation l^c between partials on the cross slip plane. In this work, we shall not assume $\sigma_s^c = 0$ in general. Hence the screw dislocation may not have an equilibrium (meta-stable) state after it is dissociated into the cross slip plane. However, this does not introduce any difficulties in the definition of function $E_b(\sigma_s^c, \sigma_e^c, \sigma_e^g)$, which only requires the meta-stable state to exist in the original glide plane.

In Escaig's model, the shape of the two partials on the cross-slip plane between the constriction nodes are described by two continuous curves $y_1(x)$ and $y_2(x)$, as shown in Fig. 1(b). The two constriction nodes are located on the x-axis at $\pm x_d$, so that $y_1(\pm x_d) = y_2(\pm x_d) = 0$. x_d is chosen as the reaction-coordinate of the cross slip process. The energy barrier E_b for cross slip is obtained by finding the maximum of energy E of the intermediate cross slip configuration with respect to x_d, i.e.

$$E_b(\sigma_s^c, \sigma_e^c, \sigma_e^g) = \max_{x_d} E(x_d; \sigma_s^c, \sigma_e^c, \sigma_e^g) \tag{6}$$

The energy $E(x_d)$ is measured relative to a straight screw dislocation resting entirely on the original glide plane at equilibrium width l^g. It has separate contributions from the original glide plane and the cross slip plane.[1] Let E^c be the energy contribution from the cross-slipped segment, whose shape is described by $y_1(x)$ and $y_2(x)$. Then

$$E(x_d; \sigma_s^c, \sigma_e^c, \sigma_e^g) = \min_{y_1(x), y_2(x)} E^c[y_1(x), y_2(x); x_d; \sigma_s^c, \sigma_e^c, \sigma_e^g] + E^g(\sigma_e^g) \tag{7}$$

E^g is the energy contribution from the original glide plane on which the partial dislocations also need to form constrictions. The expression for E^g has been obtained by Stroh and is given in Eq. (B.14). E^g is a function of σ_e^g but is independent of the stresses on the cross slip plane, σ_e^c and σ_s^c. If one considers the cross slip of a screw dislocation with an existing jog, which already provides a constriction point, then the E^g term can be ignored in Eq. (7). However, we shall not ignore E^g in the following since we focus on "homogeneous" cross slip of straight screw dislocations without any jogs.

The energy contribution from the segment on the cross-slip plane, E^c, has three contributions:

$$E^c[y_1(x), y_2(x)] = W_1[y_1(x), y_2(x)] + W_2[y_1(x), y_2(x)] + W_3[y_1(x), y_2(x)] \tag{8}$$

where

$$W_1 = A\int_{-x_d}^{x_d} \ln\frac{l^g}{y_1(x) - y_2(x)}dx \tag{9}$$

[1] This is only possible within the line tension approximation, in which there is no long-range elastic interaction between the segment on the cross-slip plane and the segments on the original glide plane.

$$W_2 = T\int_{-x_d}^{x_d} \{\sqrt{1+(y_1'(x))^2}+\sqrt{1+(y_2'(x))^2}\}\,dx - 4Tx_d \tag{10}$$

$$W_2 \approx \frac{T}{2}\int_{-x_d}^{x_d} \{[y_1'(x)]^2+[y_2'(x)]^2\}\,dx \tag{11}$$

$$W_3 = \int_{-x_d}^{x_d} \{F_1^c y_1(x)+F_2^c y_2(x)\}\,dx - 2F^g l^g x_d \tag{12}$$

$$F_1^c = F^c - b\sigma_s^c/2 \tag{13}$$

$$F_2^c = -F^c - b\sigma_s^c/2 \tag{14}$$

W_1 represents the change of elastic (repulsion) energy between the two partials. W_2 represents the change of line energy, where T is the (constant) line energy per unit length. Eq. (11) is valid under the small slope approximation ($|y_1'(x)|\ll 1$ and $|y_2'(x)|\ll 1$), which is used by Stroh (1954) and Escaig (1968). We will avoid this approximation in our numerical solution in Sections 2.2 and 2.3. W_3 represent the change in stacking fault energy and work done by the stress components on the cross-slip plane. The last term in Eq. (12) is present because the energy is measured relative to the reference configuration in which the two partials are separated by l^g on the original glide plane.

Under the boundary condition that $y_1(\pm x_d) = y_2(\pm x_d) = 0$, the shape of $y_1(x)$ and $y_2(x)$ in the domain $[-x_d, x_d]$ is the one that minimizes the functional E^c. By requiring the variational derivatives vanish at the minimum, the solution $y_1(x)$ and $y_2(x)$ must satisfy the following equations (under the small slope approximation):

$$-\frac{A}{y_1(x)-y_2(x)} + F_1^c - Ty_1''(x) = 0 \tag{15}$$

$$\frac{A}{y_1(x)-y_2(x)} + F_2^c - Ty_2''(x) = 0 \tag{16}$$

These two equations can be decoupled by defining $y(x) \equiv (y_1(x)-y_2(x))/2$ and $\bar{y}(x) \equiv (y_1(x)+y_2(x))/2$. $y(x)$ describes the separation between the two partials (i.e. local half width of the stacking fault) and $\bar{y}(x)$ is the average position of the two partials (i.e. the overall shape of the perfect dislocation). They satisfy the following (independent) equations:

$$-\frac{A}{2y(x)} + F^c - Ty''(x) = 0 \tag{17}$$

$$\bar{F}^c - T\bar{y}''(x) = 0 \tag{18}$$

where

$$\bar{F}^c \equiv (F_1^c + F_2^c)/2 = -b\sigma_s^c/2 \tag{19}$$

The solution to $\bar{y}$ is easily obtained:

$$\bar{y}(x) = (x^2 - x_d^2)\bar{F}^c/(2T) \tag{20}$$

The solution to $y(x)$, on the other hand, is more difficult to obtain. Stroh (1954) obtained the solution of Eq. (17), in which $x(y)$ is expressed as an integral (see Appendix B). Stroh (1954) also obtained the integral expression for the energy when the Schmid stress is zero (see Appendix B). Based on Stroh's results, Escaig (1968) searched for the energy barrier for cross slip by finding the energy maximum in Eq. (6). Unfortunately, Escaig had to introduce several approximations to make the analytic derivation tractable. In the following, we will deviate from Escaig's approach, and solve the line tension model numerically, in order to avoid making approximations whose errors are difficult to quantify.

2.2. Numerical method

Similar to the finite element method, in our numerical method, the functions $y_1(x)$ and $y_2(x)$ are discretized by piecewise linear segments, and the minimum of energy functional $E^c[y_1(x), y_2(x); x_d]$ is searched within the space of piecewise linear functions. An advantage of this approach is that the energy is obtained simultaneously as $y_1(x)$ and $y_2(x)$ are determined. In addition, the numerical solution is valid for arbitrarily large σ_e^c, whereas Escaig's analytic solution requires $l^c > 0$, which limits the magnitude of the Escaig stress that can be applied on the cross slip plane.

The functions $y_1(x)$ and $y_2(x)$ are discretized over the domain $[-x_d, x_d]$ on a uniform grid, $x_i = -x_d + i\Delta x$, where $\Delta x = 2x_d/N$, $i = 0, \ldots, N$. Define $y_i^{(1)} \equiv y_1(x_i)$, $y_i^{(2)} \equiv y_2(x_i)$. Note $y_0^{(1)} = y_N^{(1)} = y_0^{(2)} = y_N^{(2)} = 0$. We then constrain the function $y_1(x)$ to be piecewise linear, and passing through points $(x_i, y_i^{(1)})$, and similarly for function $y_2(x)$. Under such constraints, energy functional $E^c[y_1(x), y_2(x)]$ becomes an ordinary function E_{num}^c of the array $\{y_i^{(1)}, y_i^{(2)}\}$, which is given in Appendix A. The array $\{y_i^{(1)}, y_i^{(2)}\}$ that minimizes the energy function E_{num}^c is obtained using the conjugate gradient relaxation method.

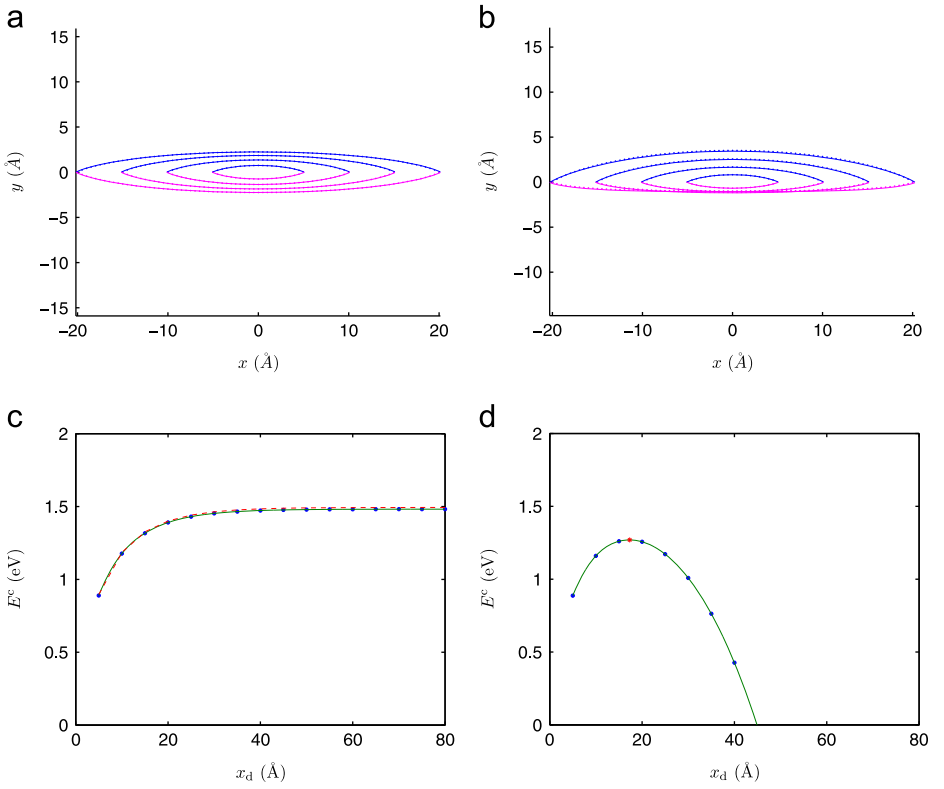

Fig. 2. (a) Equilibrium shape of the two partial dislocations on the cross slip plane under zero stress for different separations (x_d) between the constriction nodes. Dots correspond to numerical results from conjugate gradient relaxation of the discretized energy function. Lines correspond to analytic expressions by Stroh (1954). (b) Equilibrium shape of the two partial dislocations on the cross slip plane with $\sigma_s^c = 500$ MPa, and $\sigma_e^c = \sigma_e^g = 0$. (c) Energy contribution E^c from the cross-slip plane as a function of x_d under zero stress. Solid line (with dots) corresponds to numerical results from conjugate gradient relaxation. Dashed line corresponds to analytic results from Stroh (1954). (d) Numerical results of E^c as a function of x_d under stress $\sigma_s^c = 500$ MPa, and $\sigma_e^c = \sigma_e^g = 0$. The maximum energy is marked with a star.

2.3. Results

Here we present the results from the line tension model with parameters chosen to represent FCC metal Ni. The values of the parameters are given below, and their justifications based on the interatomic potential model for Ni will be presented in Section 3.2. The effective isotropic elastic constants are: shear modulus $\mu = 75.2$ GPa and Poisson's ratio $\nu = 0.376$. The magnitude of the Burgers vector is $b = a_0/\sqrt{2}$ where $a_0 = 3.52$ Å is the lattice constant. The stacking fault energy is $\gamma_{SF} = 119\ \mathrm{mJ/m^2}$. The line tension is set to $T = \alpha\mu b^2/2$, where α is empirically set to 0.45. The choice of α is discussed extensively in Section 3.2. For consistency, we choose $\Delta x = 0.5$ Å in all the following numerical calculations. We have confirmed that this choice of Δx is sufficiently small for the numerical discretization error to be negligible. For numerical efficiency, an even smaller Δx is not used.

Fig. 2(a) shows the equilibrium shape of the partial dislocations on the cross slip plane under zero stress for different separations (x_d) between the constriction nodes. The numerical results from conjugate gradient relaxation (dots) are superimposed on the analytic expression (lines) by Stroh. The energy contribution E^c from the cross slip plane as a function of x_d is plotted in Fig. 2(c). The numerical results agrees with Stroh's analytic expressions within 1% (or 0.012 eV). This small discrepancy is caused by the slight difference in the line energy term W_2 in the analytical (invoking the small slope approximation) and numerical formulation (without the small slope approximation) as well as numerical discretization error. Here $E^c(x_d)$ does not have a maximum, which is expected because there is no driving force for cross slip. The value of E^c in the limit of $x_d \to \infty$ (under zero stress) also equals the energy contribution E^g from the original glide plane (see Eqs. (7) and (B.14)). In this example, $E^g = 1.48$ eV.

Fig. 2(b) shows the equilibrium shape of the partial dislocations when $\sigma_s^c = 500$ MPa, and $\sigma_e^c = \sigma_e^g = 0$. Fig. 2(d) shows the corresponding energy contribution E^c from the cross slip plane. In this case, the function $E^c(x_d)$ has a maximum, which contributes to the energy barrier E_b for cross slip.

The numerical algorithm is so efficient that $\max_{x_d} E^c(x_d)$ for each stress condition can be obtained in about 5 s using Matlab running on a PC. Therefore, the energy barrier for a large number of stress conditions can be quickly predicted using the line tension model. The plots of E_b as a function of σ_s^c, σ_e^c, and σ_e^g, individually when the other two stresses are zero, are given in Section 3 and Fig. 6, together with predictions from the atomistic model. The Schmid and Escaig stress components

on the cross slip plane, σ_s^c and σ_e^c, are found to have comparable effects on the energy barrier. It may be puzzling how we can arrive at a different conclusion from Escaig, even though we are using essentially the same line tension model as Escaig's. The reason is that in his analytic derivation, Escaig reasoned that the effect of σ_s^c must be second order. For sufficiently small σ_s^c this must be the case, because E_b is an even function of σ_s^c in the line tension model. However, Fig. 6(a) shows that in the relevant stress range, an expansion of E_b up to the second order of σ_s^c is inadequate. In fact, E_b has deviated substantially from a quadratic function of σ_s^c at stresses as low as 200 MPa.

3. Atomistic model

3.1. Simulation set-up

We describe the inter-atomic interaction using an embedded-atom method (EAM) potential for Ni. The potential was developed based on the Voter and Chen format. It has been used by Rao et al. (2010, 1999) and has been labeled 'vnih'. We choose this potential model because the stacking fault energy it predicts (119 mJ/m^2) is in good agreement with the first principles prediction (110 mJ/m^2) and experimental measurements (125–128 mJ/m^2) (Kibey et al., 2007; Siegel, 2005). The simulation cell is initially created as a perfect FCC crystal consisting of 345,600 Ni atoms with dimensions $30[1\bar{1}0] \times 30[111] \times 20[\bar{1}\bar{1}2]$ along x-, y-, z-axes, respectively, with a lattice constant $a_0 = 3.52$ Å. The simulation cell is subjected to periodic boundary conditions along x and z, and is subjected to traction-free boundary condition along y, i.e. on the top and bottom (111) planes. Three atomistic structures, subsequently referred to as States A, B, and B′, are prepared starting from the perfect crystal, all containing a left-handed screw (LHS) dislocation along the x-axis. The Burgers vector of the perfect dislocation is $\mathbf{b} = a_0[\bar{1}10]/2$ when the line direction ξ is chosen to be along the positive x-axis. In State A, the screw dislocation dissociates onto the (111) plane, which is considered the (original) glide plane (g). In State B, the screw dislocation dissociates onto the $(11\bar{1})$ plane, which is considered the cross slip plane(c). The Burgers vectors of the partial dislocations in States A and B are given in the notation of Thompson tetrahedron in Fig. 3. In State B′, the screw dislocation has a portion dissociated onto the cross slip plane while the rest dissociates onto the original glide plane. After initialization, the atomistic structures in States A and B are relaxed to the local energy minimum using the conjugate gradient algorithm. The structure in State B′ is relaxed only for about 50 steps because it is an unstable structure and would go to either State A or B if the relaxation continues for too long. We note that while the x-axis in the atomistic model matches that in the line tension model, the y-axes in the two models do not match.

From the direction of the partial Burgers vectors, we can determine the relationship between the stress components expressed in the x–y–z coordinate system and the stress components σ_s^g, σ_e^g, σ_s^c, σ_e^c defined in the line tension model. Specifically,

$$\sigma_s^g = \sigma_{xy} \tag{21}$$

$$\sigma_e^g = \sigma_{yz} \tag{22}$$

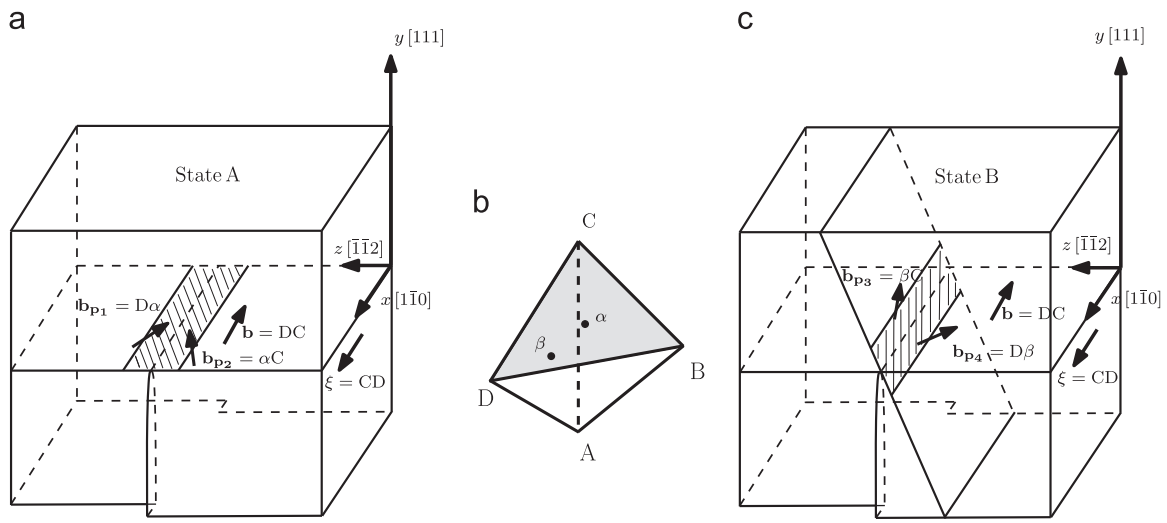

Fig. 3. Set up of the atomistic simulation cell. (a) State A contains a left-handed screw (LHS) dislocation dissociated onto the (111) plane, i.e. plane BCD in the notation of Thompson tetrahedron. The total Burgers vector is DC, when the line direction is chosen to be along the positive x-axis, i.e. $\xi = \mathrm{CD}$. The Burgers vectors of the two partials are $\mathbf{b}_{p1} = \mathrm{D}\alpha$ and $\mathbf{b}_{p2} = \alpha\mathrm{C}$. The shaded area indicates the stacking fault. (b) Thompson tetrahedron. α is the center of triangle BCD. $\beta$is the center of triangle ADC. Aα points in the positive y-direction. (c) State B contains a left-handed screw (LHS) dislocation, with the same Burgers vector as in (a), but dissociated onto the $(11\bar{1})$ plane, i.e. plane ADC. The Burgers vectors of the two partials are $\mathbf{b}_{p3} = \beta\mathrm{C}$ and $\mathbf{b}_{p4} = \mathrm{D}\beta$. The Burgers vectors of the partial dislocations are determined following the standard procedure described in Nix (2010).

$$\sigma_s^c = \frac{2\sqrt{2}\sigma_{xz} - \sigma_{xy}}{3} \tag{23}$$

$$\sigma_e^c = \frac{7\sigma_{yz} + 2\sqrt{2}(\sigma_{zz} - \sigma_{yy})}{9} \tag{24}$$

In deriving these relationships, it may be useful to note that the angle between the original glide plane and the cross slip plane is $\arccos(1/3)$. It is also important to note that the edge component of the partial dislocations point toward each other on the original glide plane, but point away from each other on the cross slip plane.

3.2. Determination of parameters in the line tension model

The parameters in the line tension model are chosen to match the behavior of the atomistic model as much as possible. From the atomistic model, we compute the stacking fault energy $\gamma_{SF} = 119$ mJ/m^2, and the cubic elastic constants: $C_{11} = 244$ GPa, $C_{12} = 149$ GPa, $C_{44} = 119$ GPa, consistent with Rao et al. (2010). Based on the anisotropic elasticity theory of dislocations (Bacon et al., 1979), we compute the energy prefactors of screw and edge dislocations on the (111) plane with line direction along $[1\bar{1}0]$, which are K_s and K_e respectively. Following the approach of Scattergood and Bacon (1975, 1982) and Yin et al. (2010), the effective isotropic elastic constants, μ and ν, are chosen by requiring $K_s = \mu b^2/(4\pi)$ and $K_e = \mu b^2/(4\pi(1-\nu))$. This leads to $\mu = 75.2$ GPa and $\nu = 0.376$.

As a benchmark for the values of μ, ν and γ_{SF} determined so far, we compare the equilibrium separation between the partial dislocations under zero stress in the line tension model and the atomistic model. In the line tension model, the equilibrium separation at zero stress is $l^g = A/\gamma_{SF}$, where A is given in Eq. (2). This leads to $l^g = 7.3$ Å. To determine the equilibrium separation in the atomistic model, we plot the central symmetry deviation (CSD) parameter for atoms immediately above and below the glide plane as a function of z in State A under zero stress. The equilibrium separation between the partials is defined as the width of the curve at half the maximum, which is $l_g^{atm} = 8.7$ Å, as shown in Fig. 4(a). The agreement between l^g (from line tension model) and l_g^{atm} is only qualitative (within 20%). The difference is caused by the spreading of the partial dislocations and their core-overlap in the atomistic model.

The only parameter in the line tension model remains to be determined is the line energy parameter α, which is a scaling parameter in the line energy $T = \alpha\mu b^2/2$. To do so we compare the shape of the partial dislocations on the cross slip plane in State B′. Because State B′ is unstable, the atomistic structure for this comparison is taken from the relaxed minimum energy path obtained in Section 3.3. Fig. 4(b) plots the positions of atoms whose CSD parameter is greater than 1 Å^2, projected onto the cross slip plane $(11\bar{1})$. The structure is taken from a simulation under stress $\sigma_{zz} = 900$ MPa, $\sigma_{yy} = -900$ MPa, other stress components being zero. This corresponds to $\sigma_e^c = 565.7$ MPa, $\sigma_s^g = \sigma_e^g = \sigma_s^c = 0$. In this configuration, the separation between the two constrictions is about $2x_d = 90$ Å. The solid lines in Fig. 4(b) are the prediction from the line tension model, using $\alpha = 0.45$. A reasonable agreement is observed between the predictions of the line tension model and the atomistic model.

This procedure does not determine the value of α uniquely. However, it does provide an estimate of the range of reasonable values for α, which is found to be between 0.1 and 0.6. In general, increasing α will decrease the separation between the partials. Significant discrepancy between line tension and atomistic predictions can be observed if α is outside the range of $[0.1, 0.6]$. Within this range, we will treat α as an empirical fitting parameter to best match the atomistic predictions of cross slip energy barriers.

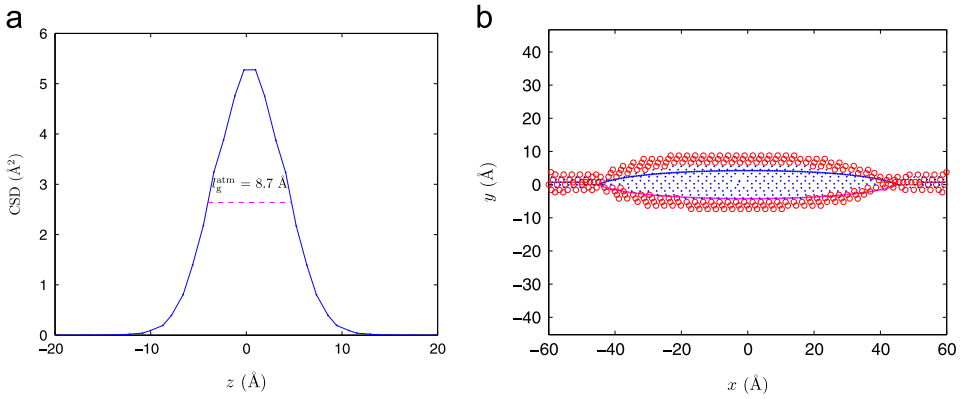

Fig. 4. (a) Central symmetry parameter of atoms in State A under zero stress as a function of z, which is a direction in the glide plane and perpendicular to the dislocation line. The width of the curve at half the maximum gives the atomistic prediction of the equilibrium splitting width $l_g^{atm} = 8.7$ Å. (b) Shape of the dislocation in State B′ projected onto the cross slip plane $(11\bar{1})$ under stress $\sigma_e^c = 565.7$ MPa, $\sigma_s^g = \sigma_e^g = \sigma_s^c = 0$. Symbols represent atoms whose CSD parameter is greater than 1.5 Å^2. Atoms whose CSD parameter is less than 3.5 Å^2 are plotted in circles, indicating the core of the partial dislocations. Other atoms are plotted as dots, indicating the stacking fault. The solid lines are predictions from the line tension model using $\alpha = 0.45$. The y-axis here is the one in the line tension model.

3.3. Results

A modified string method (Kang, 2011; Ryu et al., 2011) is used to compute the minimum energy path (MEP) between States A and B′ under stress. The length of the string is constrained to be a constant, so that the State B′ stays close enough to the saddle configuration. Without this constraint, the State B′ (i.e. the end of the path) may move very far away from the saddle configuration, especially at high stress conditions, so that the region near the saddle configuration may become poorly represented.

Fig. 5(a) plots several configurations along the MEP for cross slip under $\sigma_{xz} = -500$ MPa, other stress components being zero. The saddle configuration under this stress corresponds to ID=10. This corresponds to $\sigma_s^c = -471.4$ MPa, with $\sigma_s^g = \sigma_e^g = \sigma_e^c = 0$. In other words, the only non-zero stress in the line tension model is the Schmid stress in the cross slip plane. The saddle configuration has a segment of the dislocation dissociated onto the cross slip plane and other segments dissociated onto the original glide plane, and contains two constriction nodes, consistent with the FE mechanism. Fig. 5(b) plots the energy profile along MEP for various values of σ_{xz}. The maximum along each curve is the cross slip energy barrier for that stress.

Fig. 6(a) plots the energy barrier as a function of Schmid stress on the cross slip plane σ_s^c. The circles represent atomistic data, E_b^{atm}, and are obtained by imposing stress $\sigma_{xz} = \sigma_s^c \cdot 3/(2\sqrt{2})$, with other stress components being zero (in the x–y–z coordinate system). The line represents prediction from the line tension model, E_b^{LT}, offset by 0.7 eV. Here we use $\alpha = 0.45$ in the line tension model. The offset is needed to match the two predictions in the zero stress limit. The fact that this offset is needed is somewhat expected, because we do not expect the line tension model to be able to capture the absolute value of the energy barrier, given the multiple approximations it introduces. However, even after the offset, a discrepancy is observed in the high stress regime (>400 MPa) between the line tension model and the atomistic model, with the line tension model predicting a weaker stress dependence. Of course, the stress dependence, i.e. the slope of the energy barrier–stress curve, predicted by the line tension model can be adjusted by changing the line tension factor α. Lowering the value of α has the effect of reducing the stress dependence as well as shifting the entire energy barrier curve downward. However, the general trend observed here is unchanged if αstays within the range of $[0.1, 0.6]$.

Fig. 6(b) plots the energy barrier as a function of Escaig stress on the cross slip plane σ_e^c. The atomistic data are obtained by imposing stress $\sigma_{zz} = -\sigma_{yy} = \sigma_e^c \cdot 9/(4\sqrt{2})$, with other stress components being zero (in the x–y–z coordinate system). The

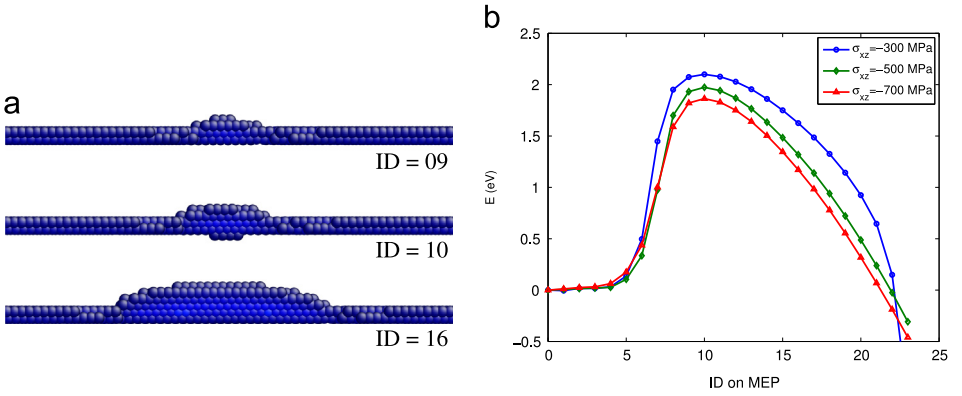

Fig. 5. (a) Atomistic configurations on the minimum energy path for cross slip at $\sigma_{xz} = -500$ MPa, other stress components being zero. This corresponds to $\sigma_s^c = -471.4$ MPa, $\sigma_s^g = \sigma_e^g = \sigma_e^c = 0$. Only atoms with CSD parameter exceeding 1 Å^2 are plotted to show the dislocation core. The viewing direction is $[\bar{1}\,\bar{1}2]$. (b) Energy profile along the minimum energy path at different values of σ_{xz}, other stress components being zero.

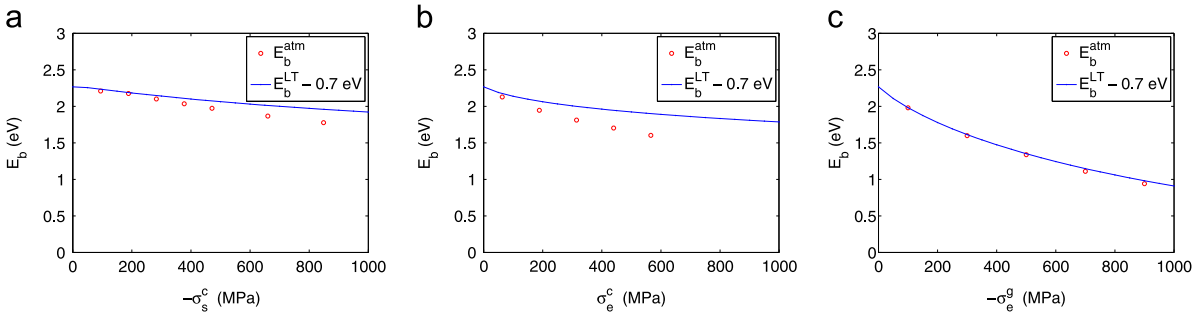

Fig. 6. Energy barrier as a function of stress. Circles represent predictions from the atomistic model, E_b^{atm}. Lines represent predictions from the line tension model offset by a constant, $E_b^{LT} - 0.7$ eV. We use $\alpha = 0.45$ in the line tension model. (a) E_b as a function of σ_s^c, with $\sigma_s^g = \sigma_e^g = \sigma_e^c = 0$. (b) E_b as a function of σ_e^c, with $\sigma_s^g = \sigma_e^g = \sigma_s^c = 0$. (c) E_b as a function of σ_e^g, with $\sigma_s^g = \sigma_s^c = \sigma_e^c = 0$.

discrepancy between the line tension model and the atomistic model is greater than that in Fig. 6(a). A significant difference is observed for σ_e^c as low as 200 MPa. Again, the atomistic model predicts a much stronger dependence on σ_e^c than the line tension model, and this trend is unchanged as long as α stays within the range of $[0.1, 0.6]$.

Fig. 6(c) plots the energy barrier as a function of Escaig stress on the original glide plane σ_e^g. The atomistic data are obtained by imposing stress $\sigma_{yz}=\sigma_e^g$, $\sigma_{yy}=-\sigma_{zz}=\sigma_e^g\cdot 7/(4\sqrt{2})$, with other stress components being zero (in the x–y–z coordinate system). Here the line tension model, with $\alpha=0.45$, predicts a stress dependence that is in good agreement with the atomistic model. The general trend does not change as along as α stays within the range of $[0.1, 0.6]$, but the offset required to match E_b^{LT} with E_b^{atm} in the zero stress limit depends on the choice of α.

3.4. Discussion

The line tension model and the atomistic model agree qualitatively with each other on the general trend in the stress effects on the cross slip energy barrier. In both models, all three stress components σ_s^c, σ_e^c, σ_e^g influence the energy barrier. The negative Escaig stress on the glide plane, $-\sigma_e^g$, compresses the width of the stacking fault on the glide plane, and is the most effective in reducing the energy barrier. The positive Escaig stress on the cross slip plane, σ_e^c, expands the width of the stacking fault on the cross slip plane, and ranks the second in the effectiveness in reducing the energy barrier. The Schmid stress on the cross slip plane, σ_s^c, makes the dislocation bow out on the cross slip plane, and reduces the energy barrier regardless of the sign of the stress. Compared to the other two stress components, σ_s^c is the least effective, but its effect is not negligible, contrary to what Escaig has assumed. Within the line tension model, the effect of two stress components on the cross slip plane, σ_s^c and σ_e^c, are comparable to each other. The atomistic model, however, predicts a more pronounced effect for both stress components, and also a larger difference in their relative effectiveness.[2]

The conclusions above are robust in the sense that in our comparison between the two models there is not much room for adjustable parameters in the line tension model. All parameters except the line tension factor α are determined directly by the interatomic potential. The parameter α need to stay within the range of $[0.1, 0.6]$ to achieve a reasonable match with the shape of the partial dislocations on the cross slip plane. The conclusions above do not change as along as α stays within this range.

Before closing this section, we wish to comment on the effect of Schmid stress on the glide plane, σ_s^g, which have been assumed to be zero throughout this paper. There is some confusion about the effect of σ_s^g in the literature. In the pioneering work of incorporating cross slip into DD models, the stress component considered by Kubin et al. (1992) was actually σ_s^g. This may seem counterintuitive because a non-zero σ_s^g would simply move the screw dislocation on its glide plane and it is not clear why it should lower the cross slip energy barrier. The paradox does not really exist because Kubin et al. (1992), following Escaig (1968), assumed the existence of (invisible) obstacles which oppose the motion of screw dislocation on the glide plane. The cross slip energy barrier is reduced by an externally applied σ_s^g because it reduces the equilibrium separation between the two partials piling against the obstacle. In this sense, the Schmid stress σ_s^g is playing a role similar to that of the Escaig stress σ_e^g. In DD simulations where all obstacles (other dislocations or inclusions) are treated explicitly, the Schmid stress σ_s^g must locally vanish on the screw dislocation when it stops moving on its glide plane and waits for cross slip. The scenario envisioned by Kubin et al. (1992) and Escaig (1968) can still be accounted for within this framework by letting the energy barrier depend on the local stress gradient. Introducing a stress gradient is a relatively straightforward generalization in the line tension model, and is perhaps feasible in the atomistic model as well.

4. Summary and outlook

We have shown that when Escaig's line tension model is solved numerically, both Escaig stress and Schmid stress have non-negligible effects on the cross slip energy barrier. In fact, the effect of Escaig stress and Schmid stress on the cross slip plane are comparable to each other. The negative Escaig stress on the original glide plane is the most effective in reducing the energy barrier, followed by the positive Escaig stress on the cross slip plane. The Schmid stress on the cross slip plane reduces the energy barrier regardless of its sign, although its effect is somewhat weaker than the Escaig stress on the cross slip plane. This general trend is consistent with the predictions of the atomistic model. However, the atomistic model predicts a more pronounced effect from the stress components on the cross slip plane than the line tension model.

A natural question to ask is: What causes the line tension model to underestimate the effect of the two stress components on the cross slip plane? Generally speaking, the line tension model can be improved in two ways. The first is to account for elastic interactions between dislocation segments (Martinez et al., 2008). The second is to allow the Burgers vector of the cross slip segment to be a variable during the cross slip process (Ramirez et al., 2012). We note that cross slip may be viewed as heterogeneous dislocation nucleation on the cross slip plane, assisted by the dislocation on the original glide plane. For the case of homogeneous dislocation nucleation, it has been found that allowing the dislocation Burgers vector to grow during the nucleation process is important for correctly capturing the nucleation barrier (Aubry et al., 2011).

[2] The atomistic model also predicts that a sufficiently high Schmid stress, σ_s^c, can reduce the cross slip activation energy to zero, through the Fleischer mechanism (Cai et al., 2004). However, the FE mechanism is observed for all the stress conditions considered in this work. In other words, the stress values here ($\sigma_s^c < 1$ GPa) are still insufficient for the Fleischer mechanism.

Hence it seems likely that including the Burgers vector in the reaction coordinate may improve the dependence of the energy barrier on the stress on the cross slip plane. It is of interest to find out which approach would improve the stress dependence of the activation energy.

Another approximation in the line tension model considered here is that the line energy is assumed to be a constant independent of dislocation orientation. Even within the line tension approximation, a more realistic description is to allow the line energy per unit length to depend on the dislocation character angle, with the edge orientation having a higher energy than the screw orientation. An orientation-dependent line energy model has been shown to provide a more physical description of dislocations (Koehler and de Wit, 1959; Cash and Cai, 2011) than the constant line tension model. When the line energy is assumed to be a constant, the line tension model predicts that the two constrictions have the same structure and make the same contribution to the energy barrier. However, atomistic simulations have shown that the two constrictions have different structures and energy contributions (Rasmussen et al., 1997). This behavior can be accounted for by introducing an orientation dependent line energy. This extension of the line tension would make analytic solution of the cross slip energy barrier nearly impossible, but poses no major difficulty in the numerical solution.

The goal of our work in this direction is the construction of the cross slip energy barrier E_b as a function of all relevant stress components, and perhaps stress gradients. Given the number of relevant stress components, a large number of atomistic calculations (MEP searches) would be necessary if this function is to be constructed from atomistic model alone. Such an approach would be quite challenging, but not infeasible given the computational capabilities today. Alternatively, one may develop a coarse-grained model, such as the line tension model considered here, that is computationally more efficient than the atomistic model, but can be fitted to the predictions of atomistic model. If successful, this approach would reduce the number of independent energy barrier calculations using the expensive atomistic model. Finally, we mention in passing that, when predicting the cross slip rate, we ultimately need to know the activation free energy $F_b = E_b - TS_b$, where E_b is the activation energy considered here. S_b is the activation entropy, which still need to be quantified (Ryu et al., 2011).

Acknowledgement

This work was supported by the U.S. Department of Energy, Office of Basic Energy Sciences, Division of Materials Sciences and Engineering under Award No. DE-SC0010412 (W.C.).

Appendix A. Discretized energy function and derivatives

The discretized version of the energy functional $E^c[y_1(x), y_2(x)]$ is an ordinary function of the nodal positions, i.e.,

$$E^c_{num}(\{y_i^{(1)}, y_i^{(2)}\}) = A\sum_{i=0}^{N-1}(\ln l^g - f(y_i^{(1)} - y_i^{(2)}, y_{i+1}^{(1)} - y_{i+1}^{(2)}))\Delta x + T\sum_{i=0}^{N-1}\sqrt{(y_{i+1}^{(1)} - y_i^{(1)})^2 + (\Delta x)^2} - 2Tx_d + T\sum_{i=0}^{N-1}\sqrt{(y_{i+1}^{(2)} - y_i^{(2)})^2 + (\Delta x)^2} - 2Tx_d + \sum_{i=1}^{N-1}(F_1 y_i^{(1)} + F_2 y_i^{(2)})\Delta x - 2F^g l^g x_d \tag{A.1}$$

where

$$f(a,b) \equiv \int_0^1 \ln|a(1-t) + bt|\, dt = \frac{a\ln a - b\ln b}{a-b} - 1 \tag{A.2}$$

Note that for numerical robustness, in the line energy term above we have not invoked the small slope approximation, unlike Eq. (11). Whether or not the small slope approximation is used has a negligible effect on the cross slip energy, as can be seen in Fig. 2(c). The energy derivatives are the following:

$$\frac{\partial E^c_{num}}{\partial y_i^{(1)}} = -A\left[g\left(y_i^{(1)} - y_i^{(2)}, y_{i+1}^{(1)} - y_{i+1}^{(2)}\right) + g\left(y_i^{(1)} - y_i^{(2)}, y_{i-1}^{(1)} - y_{i-1}^{(2)}\right)\right]\Delta x + T\left[\frac{y_i^{(1)} - y_{i+1}^{(1)}}{\sqrt{(y_{i+1}^{(1)} - y_i^{(1)})^2 + (\Delta x)^2}} + \frac{y_i^{(1)} - y_{i-1}^{(1)}}{\sqrt{(y_{i-1}^{(1)} - y_i^{(1)})^2 + (\Delta x)^2}}\right] + F_1\Delta x \tag{A.3}$$

$$\frac{\partial E^c_{num}}{\partial y_i^{(2)}} = A\left[g\left(y_i^{(1)} - y_i^{(2)}, y_{i+1}^{(1)} - y_{i+1}^{(2)}\right) + g\left(y_i^{(1)} - y_i^{(2)}, y_{i-1}^{(1)} - y_{i-1}^{(2)}\right)\right]\Delta x + T\left[\frac{y_i^{(2)} - y_{i+1}^{(2)}}{\sqrt{(y_{i+1}^{(2)} - y_i^{(2)})^2 + (\Delta x)^2}} + \frac{y_i^{(2)} - y_{i-1}^{(2)}}{\sqrt{(y_{i-1}^{(2)} - y_i^{(2)})^2 + (\Delta x)^2}}\right] + F_2\Delta x \tag{A.4}$$

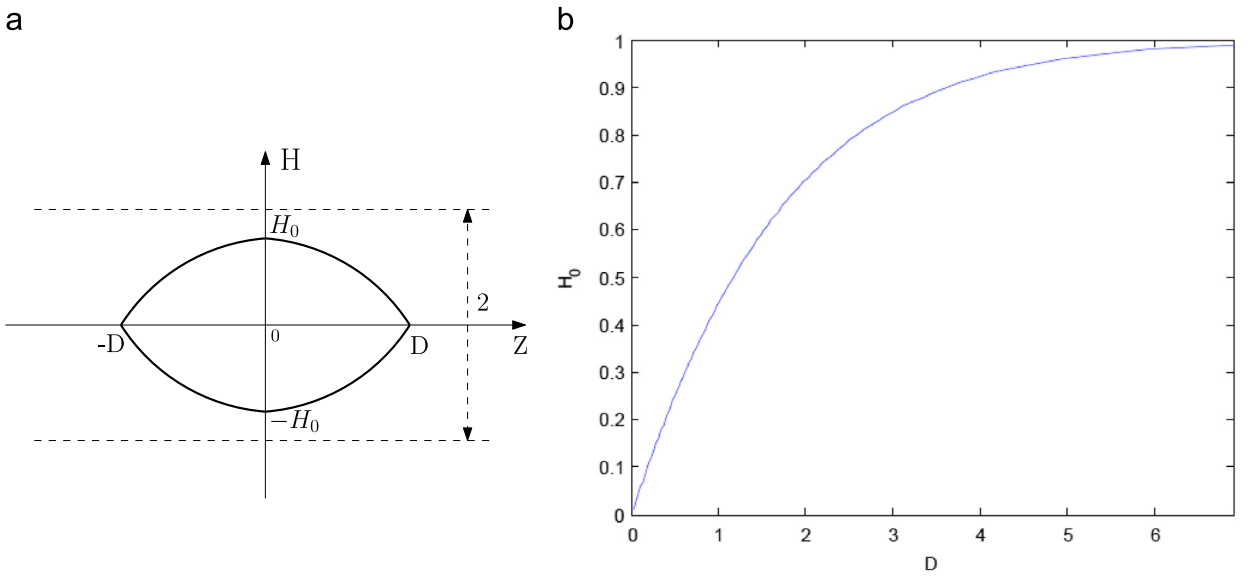

Fig. B1. (a) Two partials on a plane (the cross slip plane in Escaig's model) with two constriction points in the dimensionless Z –H space. (b) H_0 as a function of D.

where

$$g(a,b) \equiv \frac{\partial f(a,b)}{\partial a} = \frac{(a-b)-b(\ln a - \ln b)}{(a-b)^2} \tag{A.5}$$

Appendix B. Analytic solution by Stroh

We start with Stroh's equation of equilibrium, i.e. Eq. (17)

$$T\frac{d^2y}{dx^2} + \frac{A}{2y} - F^c = 0 \tag{B.1}$$

Recall $l^c = A/F^c$ is the equilibrium separation between the partials on the cross-slip plane. The equation can be rewritten as

$$T\frac{d^2y}{dx^2} + \frac{A}{2y} - \frac{A}{l^c} = 0 \tag{B.2}$$

Through the definition of dimensionless quantities

$$H \equiv \frac{2y}{l^c} \tag{B.3}$$

$$Z \equiv \frac{2x}{l^c}\left(\frac{A}{T}\right)^{1/2} \tag{B.4}$$

the equation can be rewritten as

$$2\frac{d^2H}{dZ^2} = 1 - \frac{1}{H} \tag{B.5}$$

The shape of the partial dislocations in terms of dimensionless variables is illustrated in Fig. B1(a). By symmetry, the boundary condition for $y(x)$ in the domain $[0, x_d]$ is

$$y = y_0, \quad dy/dx = 0, \quad \text{at } x = 0 \tag{B.6}$$

$$y = 0, \quad \text{at } x = x_d \tag{B.7}$$

which can be expressed in terms of dimensionless variables as

$$H = H_0, \quad dH/dZ = 0, \quad \text{at } Z = 0 \tag{B.8}$$

$$H=0, \quad \text{at } Z=D \tag{B.9}$$

where $H_0=2y_0/l^c$, $D=2x_d(A/T)^{1/2}/l^c$, $Z=2x(A/T)^{1/2}/l^c$.

Stroh (1954) obtained the following solution for Eq. (B.5):

$$Z=H_0\int_{H/H_0}^{1}[-\ln t+H_0(t-1)]^{-1/2}\,dt \tag{B.10}$$

Eq. (B.10) is essentially an integral expression of $x(y)$, since $Z\propto x$ and $H\propto y$. Given the boundary condition that $H=0$ at $Z=D$, we have

$$D=H_0\int_{0}^{1}[-\ln t+H_0(t-1)]^{-1/2}\,dt \tag{B.11}$$

Eq. (B.11) is essentially an expression of $x_d(y_0)$, since $D\propto x_d$ and $H_0\propto y_0$. The relationship between D and H_0 is plotted in Fig. B1(b). As $D\to\infty$, H_0 approaches 1. This means the separation between the two partials at $x=0$ goes to the equilibrium value l^c when the two constriction nodes are separated infinitely apart.

When Schmid stress is zero on the cross slip plane (i.e. $\sigma_s^c=0$), the shape of the two partials will be symmetric with respect to each other, i.e. $y_1(x)=-y_2(x)=y(x)$. In this case, the energy $E^c[y_1(x),y_2(x)]$ can be written as a functional of $y(x)$. Plugging in the equilibrium solution of $x(y)$ as given by Eq. (B.10), we have

$$E^c=2Ax_d\ln(l^g/l^c)-2Fx_d(l^g-l^c)+l^c(AT)^{1/2}H_0 \times\left[2\int_0^1[-\ln t+H_0(t-1)]^{1/2}\,dt+\int_0^1\frac{-\ln H_0+H_0-1}{[-\ln t+H_0(t-1)]^{1/2}}dt\right] \tag{B.12}$$

In the limit of $x_d\to\infty$, $H_0\to 1$, we have

$$\lim_{x_d\to\infty}E^c=2Ax_d\ln(l^g/l^c)-2Fx_d(l^g-l^c)+2l^c(AT)^{1/2}\int_0^1[-\ln t+(t-1)]^{1/2}\,dt \tag{B.13}$$

The same analysis can be applied to the two semi-infinite dislocation segments on the original glide plane. Their energy contribution is

$$E^g=2l^g(AT)^{1/2}\int_0^1[-\ln t+(t-1)]^{1/2}\,dt \tag{B.14}$$

This is the energy cost of producing an isolated constriction node on an otherwise perfectly straight screw dislocation, as given by Eq. (10) of Stroh (1954).

References

Arsenlis, A., Cai, W., Tang, M., Rhee, M., Oppelstrup, T., Hommes, G., Pierce, T.G., Bulatov, V.V., 2007. Enabling strain hardening simulations with dislocation dynamics. Model. Sim. Mater. Sci. Eng. 15, 553.

Aubry, S., Kang, K., Ryu, S., Cai, W., 2011. Energy barrier for homogeneous dislocation nucleation: comparing atomistic and continuum models. Script. Mater. 64, 1043.

Bacon, D.J., Barnett, D.M., Scattergood, R.O., 1979. Anisotropic continuum theory of lattice defects. Prog. Mater. Sci. 23, 51262.

Bonneville, J., Escaig, B., 1979. Cross-slipping process and the stress-orientation dependence in pure copper. Acta Metall. 27, 1477.

Bonneville, J., Escaig, B., Martin, J.L., 1988. A study of cross-slip activation parameters in pure copper. Acta Metall. 36, 1989.

Bulatov, V.V., Cai, W., 2006. Computer Simulations of Dislocations. Oxford University Press.

Cai, W., Bulatov, V.V., Justo, J.F., Yip, S., Argon, A.S., 2000. Intrinsic mobility of a dissociated dislocation in silicon. Phys. Rev. Lett. 84, 3346.

Cai, W., Bulatov, V.V., Chang, J., Li, J., Yip, S., 2004. Dislocation core effects on mobility. In: Nabarro, F.R.N., Hirth, J.P. (Eds.), Dislocations in Solids, vol. 12. North-Holland, Amsterdam, pp. 1.

Cash, W.D., Cai, W., 2011. Dislocation contribution to acoustic nonlinearity: the effect of orientation dependent line energy. J. Appl. Phys. 109, 014915.

Escaig, B., 1968. Sur le Glissement Dévié des Dislocations Dans la Structure Cubique a Faces Centrées. J. Phys. 29, 225.

Jackson, P.J., 1985. Dislocation modelling of shear in F.C.C. crystals. Prog. Mater. Sci. 29, 139.

Kang, K., 2011. Atomistic Modelling of Fracture Mechanisms in Semiconductor Nanowires Under Tension (Ph.D. thesis). Stanford University.

Kibey, S., Liu, J.B., Johnson, D.D., Sehitoglu, H., 2007. Predicting twinning stress in fcc metals: linking twin-energy pathways to twin nucleation. Acta Mater. 55, 6843.

Koehler, J.S., de Wit, G., 1959. Influence of elastic anisotropy on the dislocation contribution to the elastic constants. Phys. Rev. 116, 1121.

Kubin, L.P., Canova, G., Condat, M., Devincre, B., Pontikis, V., Brechet, Y., 1992. Dislocation microstructures and plastic flow: a 3D simulation. Solid State Phenomena 23 and 24, 455.

Martinez, E., Marian, J., Arsenlis, A., Victoria, M., Perlado, J.M., 2008. Atomistically informed dislocation dynamics in fcc crystals. J. Mech. Phys. Solids 56, 869.

Nix, W.D., 2010. Partial Dislocation Tutorial for FCC Metals. ⟨http://www.imechanica.org/node/7334⟩.

Puschl, W., 2002. Models for dislocation cross-slip in close-packed crystal structures: a critical review. Prog. Mater. Sci. 47, 415.

Puschl, W., Schoeck, G., 1993. Calculation of cross-slip parameters in FCC crystals. Mater. Sci. Eng. A 164, 286.

Ramirez, B.R., Ghoniem, N., Po, G., 2012. Ab initio continuum model for the influence of local stress on cross-slip of screw dislocations in fcc metals. Phys. Rev. B 86, 094115.

Rao, S., Parthasarathy, T.A., Woodward, C., 1999. Atomistic simulation of cross-slip processes in model fcc structures. Philos. Mag. A 79, 1167.

Rao, S.I., Dimiduk, D.M., El-Awady, J.A., Parthasarathy, T.A., Uchic, M.D., Woodward, C., 2010. Activated states for cross-slip at screw dislocation intersection in face-centered cubic nickel and copper via atomistic simulation. Acta Mater. 58, 5547.

Rasmussen, T., Jacobsen, K.W., Leffers, T., Pedersen, O.B., 1997. Simulations of the atomic structure, energetics, and cross slip of screw dislocations in copper. Phys. Rev. B 56, 2977.

Ryu, S., Kang, K., Cai, W., 2011. Entropic effect on the rate of dislocation nucleation. Proc. Natl. Acad. Sci. 108, 5174.

Scattergood, R.O., Bacon, D.J., 1975. The Orowan mechanism in anisotropic crystals. Philos. Mag. 31, 179.
Scattergood, R.O., Bacon, D.J., 1982. The strengthening effect of voids. Acta Metall. 30, 1665.
Siegel, D.J., 2005. Generalized stacking fault energies, ductilities, and twinnabilities of Ni and selected Ni alloys. Appl. Phys. Lett. 87, 121901.
Stroh, A.N., 1954. Constrictions and jogs in extended dislocations. Proc. Phys. Soc. B 67, 427.
Suresh, S., 2004. Fatigue of Materials, second ed. Cambridge University Press.
Vegge, T., Rasmussen, T., Leffers, T., Pedersen, O.B., Jacobsen, K.W., 2001. Atomistic simulations of cross-slip of jogged screw dislocations in copper. Philos. Mag. Lett. 81, 137.
Washburn, J., 1965. Intersection cross slip. Appl. Phys. Lett. 7, 183.
Yin, J., Barnett, D.M., Cai, W., 2010. Efficient computation of forces on dislocation segments in anisotropic elasticity. Model. Sim. Mater. Sci. Eng. 18, 045013.